J Biomol NMR (2014) 60:231–240
DOI 10.1007/s10858-014-9872-9

ARTICLE

A six-dimensional alpha proton detection-based APSY experiment for backbone assignment of intrinsically disordered proteins

Xuejun Yao · Stefan Becker · Markus Zweckstetter

Received: 8 September 2014 / Accepted: 30 October 2014 / Published online: 4 November 2014

Abstract Sequence specific resonance assignment is the prerequisite for the NMR-based analysis of the conformational ensembles and their underlying dynamics of intrinsically disordered proteins. However, rapid solvent exchange in intrinsically disordered proteins often complicates assignment strategies based on HN-detection. Here we present a six-dimensional alpha proton detection-based automated projection spectroscopy (APSY) experiment for backbone assignment of intrinsically disordered proteins. The 6D HCACONCAH APSY correlates the six different chemical shifts, $H_\alpha(i-1)$, $C_\alpha(i-1)$, $C'(i-1)$, N(i), $C_\alpha(i)$ and $H_\alpha(i)$. Application to two intrinsically disordered proteins, 140-residue α-synuclein and a 352-residue isoform of Tau, demonstrates that the chemical shift information provided by the 6D HCACONCAH APSY allows efficient backbone resonance assignment of intrinsically disordered proteins.

Keywords NMR · Intrinsically disordered protein · Assignment · α-Synuclein · APSY · Solvent exchange

Electronic supplementary material The online version of this article (doi:10.1007/s10858-014-9872-9) contains supplementary material, which is available to authorized users.

X. Yao · S. Becker · M. Zweckstetter (✉)
Department for NMR-based Structural Biology, Max Planck Institute for Biophysical Chemistry, 37077 Göttingen, Germany
e-mail: mzwecks@gwdg.de; markus.zweckstetter@dzne.de

M. Zweckstetter
German Center for Neurodegenerative Diseases (DZNE), Göttingen, 37077 Göttingen, Germany

M. Zweckstetter
Center for Nanoscale Microscopy and Molecular Physiology of the Brain, University Medical Center Göttingen, 37075 Göttingen, Germany

Introduction

It is estimated that in eukaryotic organisms intrinsically disordered proteins (IDPs)—proteins which lack a rigid secondary and tertiary structure—constitute approximately 30 % of all proteins (Uversky 2002). IDPs play important roles in a variety of biological processes including transcriptional regulation, translation and cellular signal transduction (Iakoucheva et al. 2002; Tompa 2002; Wright and Dyson 1999). In addition, several neurodegenerative disorders such as Alzheimer's disease and Parkinson's disease are characterized by a pathogenic process in which IDPs aggregate into toxic oligomers and amyloid fibrils (Uversky 2011). Moreover, IDPs are enriched in proteins associated with human diseases such as cancer, cardiovascular disease and diabetes, making IDPs novel and interesting drug targets (Uversky et al. 2008).

A number of biophysical techniques can be employed to investigate disordered proteins. For example, small angle X-ray scattering and pulsed field gradient NMR studies of IDPs showed that the hydrodynamic radius of IDP molecules is larger than that of globular folded proteins with the same molecular weight, but is still smaller than the value estimated for a random coil protein of the same size (Wilkins et al. 1999). Due to their inherent plasticity IDPs are not amenable to structural characterization by X-ray crystallography. This makes NMR spectroscopy the only method that provides residue-specific insights into the conformational ensembles populated by IDPs in solution and their associated exchange dynamics (Jensen et al. 2013; Rezaei-Ghaleh et al. 2012; Uversky 2002).

A prerequisite for the NMR-based analysis of IDPs is their sequence specific resonance assignment. In order to achieve the resonance assignment of IDPs, three-dimensional HN-detected triple-resonance experiments, which

are commonly used for globular proteins, might be employed. These experiments are in principle of high sensitivity due to the favorable spin relaxation properties in IDPs—a consequence of their pronounced flexibility. At the same time they suffer from several limitations in the case of IDPs, such as small chemical shift dispersion due to the efficient averaging of the chemical environment and a high sequence degeneracy (Mittag and Forman-Kay 2007). Furthermore, amide protons of IDPs are barely protected from exchange with water due to the lack of hydrogen bonds, leading to severe line broadening at high temperature and pH values above ~6.2 (Croke et al. 2008). In addition, IDPs often contain many proline residues (Marsh and Forman-Kay 2010), which are not observable in HN-detected experiments and lead to gaps in the sequential assignment.

Various strategies have been designed to overcome these limitations. Signal overlap can be reduced by introduction of additional chemical shift evolution periods in four to seven-dimensional triple-resonance experiments (Atreya and Szyperski 2004; Coggins et al. 2004; Fiorito et al. 2006; Hiller et al. 2005; Kazimierczuk et al. 2013; Kim and Szyperski 2003; Kupce and Freeman 2003a, b, 2004; Motackova et al. 2010; Narayanan et al. 2010; Shen et al. 2005; Szyperski and Atreya 2006; Zawadzka-Kazimierczuk et al. 2012b). For example, a combination of five-, six- and seven-dimensional HN-detected experiments, which were recorded using automated projection spectroscopy (APSY; Hiller et al. 2005) in combination with the assignment software MARS (Jung and Zweckstetter 2004), allowed automatic assignment of 92 % of the assignable residues of the 441-residue IDP Tau (Narayanan et al. 2010). In addition, ^{13}C-detection is a very powerful approach to increase signal dispersion and reduce line broadening, which is either caused by solvent exchange or conformational exchange (Felli and Brutscher 2009; Skora et al. 2010). ^{13}C-detected NMR experiments (Bermel et al. 2006a, b, 2012a, b; Bertini et al. 2004; Pervushin and Eletsky 2003; Shimba et al. 2004; Takeuchi et al. 2010), in particular when combined with non-uniform sampling techniques (Barna et al. 1987; Bermel et al. 2012b, 2013; Chylla and Markley 1995; Coggins and Zhou 2006; Holland et al. 2011; Kazimierczuk et al. 2006; Kazimierczuk and Orekhov 2011; Korzhneva et al. 2001; Novacek et al. 2011; Orekhov et al. 2001), can therefore enable the resonance assignment and structural characterization of large IDPs (Csizmok et al. 2008; Narayanan et al. 2010; Novacek et al. 2013; Zawadzka-Kazimierczuk et al. 2012a).

Proton alpha (HA)-detection provides an alternative approach for assignment of IDPs besides HN- and ^{13}C-detected experiments, as the resonance peaks on HA-detected spectra are not deteriorated by line broadening due to amide proton exchange and the large gyromagnetic ratio of protons provides optimal sensitivity during detection. Early on, two 2D experiments, HA(CA)N and HA(CA-CO)N, and their 3D analogs were proposed for assignment of proline-rich peptides (Wang et al. 1995). HACAN correlates both intra- and inter-residual chemical shifts (H_α(i)–C_α(i)–N(i)/N(i + 1)) while HACA(CO)N exclusively establishes inter-residue correlations (H_α(i)–C_α(i)–N(i + 1)). Moreover, residue-type information can be obtained when the $^{13}C_\beta$ chemical shift is detected in a three-dimensional (HB)CBCA(CO)N(CA)HA experiment (Kanelis et al. 2000). A proline-optimized CDCA(NCO)-CAHA has also been developed for sequential assignment of proline residues by correlating $^{13}C_\delta$ and $^{13}C_\alpha$ chemical shifts of prolines with the H_α chemical shift of the preceding residue (Bottomley et al. 1999).

Chemical shifts of $^{13}C'$ and ^{15}N are especially useful to resolve signal overlap due to their large chemical shift dispersion even for IDPs. Therefore, iH(CA)NCO and H(CA)CON experiments, which provide the intra-residual correlation $^{1}H_\alpha$(i)–^{15}N(i)–$^{13}C'$(i) and the sequential correlation $^{1}H_\alpha$(i)–$^{13}C'$(i)–^{15}N(i + 1), respectively, enable sequential assignment with efficient use of ^{15}N and $^{13}C'$ chemical shifts instead of $^{13}C_\alpha$ (Mantylahti et al. 2010). The HA-detected experiments, (HCA)CON(CA)H and (HCA)NCO(CA)H, further provide the correlation C′(i − 1)–N(i)–H_α(i), while auto-correlation peaks are suppressed (Mantylahti et al. 2011). Together with iH(CA)NCO, these experiments provide a robust platform for backbone assignment of IDPs.

Here we combine HA-detection with chemical shift co-evolution in a six-dimensional triple-resonance experiment. The experiment was designed to correlate the six different nuclei H_α(i − 1), C_α(i − 1), C′(i − 1), N(i), C_α(i) and H_α(i) (Fig. 1a) and to utilize the APSY approach to obtain highly accurate chemical shifts. Due to the high dimensionality of the experiment, signal overlap is minimized, while HA-detection avoids solvent exchange-based signal attenuation. Application of the experiment to the IDPs α-synuclein and Tau demonstrated that the sequential connectivity provided by this single experiment is sufficient to achieve a large part of the backbone resonance assignment.

Materials and methods

NMR spectroscopy

NMR samples contained 1 mM of ^{13}C/^{15}N-labeled α-synuclein in 50 mM phosphate buffer, pD 6.0, 100 mM NaCl or 1 mM of ^{13}C/^{15}N-labeled htau23 (the isoform of Tau with 352 residues) in 50 mM phosphate buffer, pD 6.8. NMR spectra were recorded at 298 K on Bruker 700 MHz (α-synuclein) and 900 MHz spectrometers (htau23)

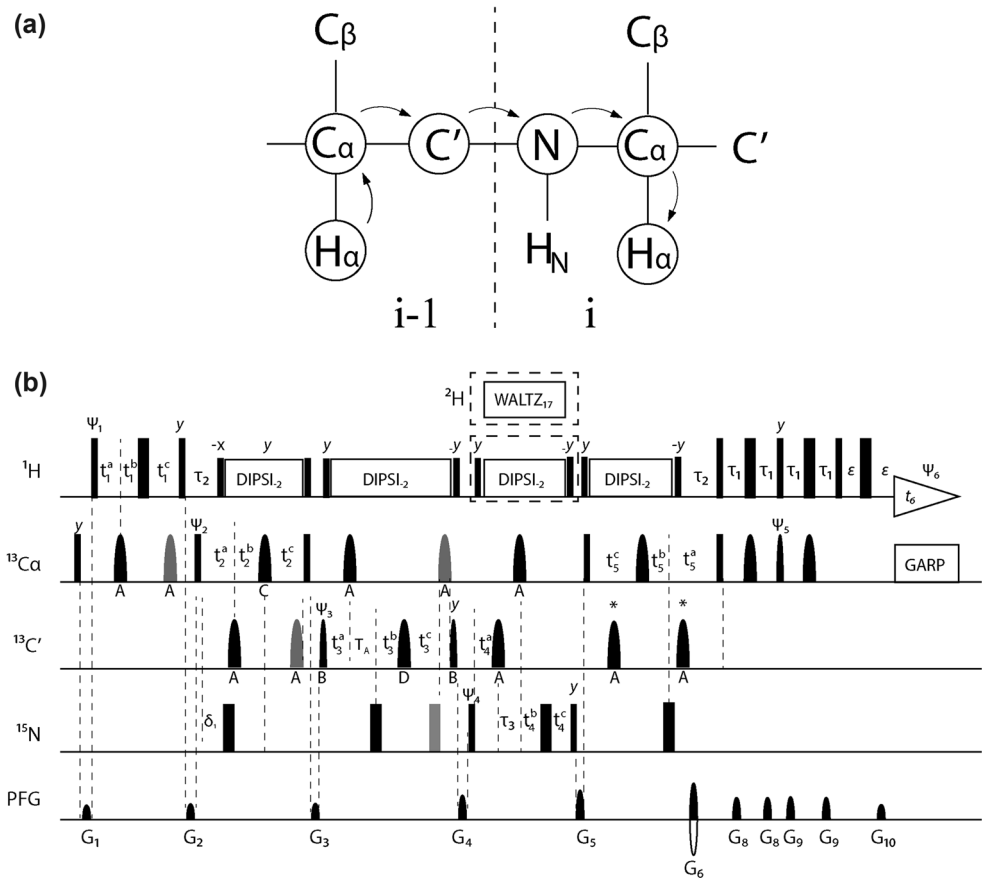

Fig. 1 6D HCACONCAH APSY. **a** Schematic presentation of the magnetization transfer pathway. **b** Pulse sequence. Radio-frequency pulses are applied at 118.0 ppm for ^{15}N, 172.5 ppm for carbonyl carbons, and 51.0 ppm for $^{13}C_{\alpha}$. *Narrow* and *wide rectangular bars* are 90° and 180° hard pulses, respectively. *Thin* (*fat*) *sine bells* are shaped 90° (180°) pulses on ^{13}C. Four different *shaped pulses* were employed (labeled *A–D*): *A* I-burp of 230 µs, *B* Gaussian shape of 410 µs, *C* RE-burp of 290 µs applied at 42.0 ppm, *D* RE-burp of 580 µs applied at 172.5 ppm. The duration of the *shaped pulses* should be adjusted for different magnet fields (here 700 MHz). The two *pulses* marked with an *asterisk* are centered with respect to the time periods t_5^c and $t_5^a + t_5^b$, respectively. *Grey pulses* are used to compensate for Bloch–Siegert effects (Mccoy and Mueller 1992). Decoupling on ^{1}H is achieved using DIPSI-2, while GARP is used for ^{13}C decoupling. If the sample is in D_2O, ^{1}H decoupling is replaced by ^{2}H decoupling using WALTZ17 (*dashed rectangle*). *Curved shapes* on the PFG line represent sine bell-shaped, pulsed magnetic field gradients applied along the z-axis. G_6 and G_{10} have a duration of 1,000 µs with gradient strengths set to $G_6/G_{10} = \gamma_H/\gamma_N$. Phase cycling follows: ψ_1 = x, ψ_2 = [x], ψ_3 = [x, x, x, x, −x, −x, −x, −x], ψ_4 = [x, −x], ψ_5 = [− y, −y, y, y], ψ_6 = [x, −x, −x, x, −x, x, x, −x] with other pulses applied along x. Constant delays were set to $T_A = 16.6$ ms, $T_{NC} = 25$ ms, $\tau_1 = 1.7$ ms, $\tau_2 = 4.8$ ms, $\tau_3 = T_{NC} - T_A = 8.4$ ms,; ε is set to 1.2 ms. The initial values of the delays, which are changed during chemical shift encoding, are: $t_1^a = t_1^c = 1.7$ ms, $t_2^a = 4.5$ ms, $t_2^b = 9.5$ ms, $t_2^c = 14$ ms, $t_3^a = t_3^b = 0$ ms, $t_3^c = 16.6$ ms, $t_4^a = 16.6$ ms, $t_4^b = 0$ ms, $t_4^c = T_{NC} = 25$ ms, $t_5^a = t_5^c = 14$ ms, $t_5^b = 0$ ms, and the delay δ_1 is adjusted to $\delta_1 = (t_2^a + t_2^b - t_2^c)/2$. In the all indirect evolution periods, semi-constant time evolution is used. Quadrature detection for the indirect dimensions is achieved for t_1, t_2, t_3 and t_4 by States-TPPI incrementation of the phases ψ_1, ψ_2, ψ_3 and ψ_4, and for t_5 by echo-anti-echo selection incrementing ψ_5 and inverting the gradient pulse G_6. The trigonometric theorem was used to obtain pure cosine and sine terms for a subsequent hypercomplex Fourier transformation (Kupce and Freeman 2004)

equipped with cryogenic probes. 65 projections from 25 angle sets were recorded in 60 and 85 h for α-synuclein and htau23, respectively. Generally, projection angles should be chosen such that projections are distributed roughly evenly in the time domain. For further details regarding practical aspects of setting up APSY experiments, please see (Hiller et al. 2008). Acquisition times in case of α-synuclein were 0.07619 s ($H_\alpha(i-1)$), 0.019048 s ($C_\alpha(i-1)$), 0.045714 s ($C'(i-1)$), 0.040816 s (N(i)) and 0.019048 s ($C_\alpha(i)$). For htau23 we used 0.084444 s ($H_\alpha(i-1)$), 0.019487 s ($C_\alpha(i-1)$), 0.050667 s ($C'(i-1)$), 0.048718 s (N(i)) and 0.019487 s ($C_\alpha(i)$).

The acquired 2D projections were processed using the program PROSA (Güntert et al. 1992). Peak picking in the projections was performed using GAPRO (Hiller et al. 2005) with the signal-to-noise threshold set to $R_{min} = 6$. Resulting peak lists were analyzed using GAPRO to generate a 6D peak list. The following GAPRO parameters for

α-synuclein were used: $S_{min,1} = S_{min,2} = 12$ (minimal supports), $r_{min} = 15$ Hz and $\Delta\nu_{min} = 5$ Hz (peak matching tolerance in the indirect and direct dimension; Hiller et al. 2008). For htau23, GAPRO was applied with the parameters $S_{min,1} = S_{min,2} = 9$, $r_{min} = 15$ Hz, $\Delta\nu_{min} = 5$ Hz.

Automatic resonance assignment using MARS

The list of unassigned 6D peaks $H_\alpha(i-1)$–$C_\alpha(i-1)$–$C'(i-1)$–$N(i)$–$C_\alpha(i)$–$H_\alpha(i)$ was fed into the assignment program MARS (Jung and Zweckstetter 2004). Multiple assignment runs were performed, in which the cutoffs for matching the chemical shift pairs $H_\alpha(i)$–$C_\alpha(i)$ and $H_\alpha(i-1)$–$C_\alpha(i-1)$ were varied. The highest number of assigned residues was obtained with cutoffs of 0.05 ppm for C_α and 0.02 ppm for H_α.

Results

Description of the pulse sequence

The 6D HCACONCAH APSY pulse sequence is based on the 3D HA-detected (HCA)CON(CA)H experiment proposed by Mantylahti et al. (2011). The pulse sequence of the 6D HCACONCAH starts with a 90° purge pulse on $^{13}C_\alpha$ (Fig. 1b). With the first ^{1}H–^{13}C INEPT, $^1H_\alpha(i-1)$ spin polarization is transferred to the covalently bonded $^{13}C_\alpha(i-1)$, while at the same time the chemical shift of $^1H_\alpha(i-1)$ is recorded. Subsequently, the coherence is transferred to $^{13}C'(i-1)$ using the one-bond scalar coupling between $^{13}C_\alpha$ and $^{13}C'$. Refocusing of anti-phase ^{1}H–^{13}C coherence is implemented in the delay τ_2, followed by ^{1}H decoupling. The shaped 180° pulse on carbon covers both the $^{13}C_\alpha$ and $^{13}C_\beta$ region, in order to keep $^1J_{C\alpha C\beta}$ active. The position of the 180° pulse on ^{15}N is adjusted for ^{15}N decoupling according to $\delta_1 = (t_2^a + t_2^b - t_2^c)/2$. Next, anti-phase $^{13}C_\alpha$–$^{13}C'$ coherence is refocused and magnetization is transferred to ^{15}N via $^1J_{C'N}$. In the following delay, the ^{15}N chemical shift is labeled and magnetization transfer to $^{13}C_\alpha(i)$ occurs. The anti-phase coherence is then refocused with respect to ^{15}N while the $^{13}C_\alpha(i)$ chemical shift evolved. Finally, magnetization is converted into observable $^1H_\alpha$ coherence by the subsequent two INEPT transfer units (Kay et al. 1992). Sequential assignment by the 6D HCACONCAH is thus established through correlation of two sequential C_α and H_α chemical shift pairs (Fig. 1a).

Chemical shift labeling in t_1, t_2, t_3, t_4 and t_5 is implemented in a semi-constant time manner to allow high resolution in the $H_\alpha(i-1)$, $C_\alpha(i-1)$, $C'(i-1)$, $N(i)$ and $C_\alpha(i)$ dimension. Most water signal is suppressed by the gradient pulses G_6 and G_{10} for coherence selection. Residual water signal may still be too large and interfere with the detection of HA signals that are close to the water resonance. In this case, the protein might be dissolved in 100 % D_2O and ^{1}H decoupling during the ^{15}N evolution period is replaced by ^{2}H decoupling (as shown by the dashed rectangle in Fig. 1b).

A critical step in the pulse sequence is the transfer of magnetization from $^{15}N(i)$ to $^{13}C_\alpha(i)$. Due to a similar magnitude of $^1J_{C\alpha N}$ and $^2J_{C\alpha N}$, the magnetization would be transferred in the forward direction to $^{13}C_\alpha(i)$, but also backward to $^{13}C_\alpha(i-1)$. This would decrease the signal of interest and increase the number of cross-peaks without providing additional information. Moreover, the two cross-peaks, which are then present from each pair of sequentially adjacent C_α groups, are difficult to distinguish by automatic assignment programs and complicate efficient resonance assignment. In order to suppress the auto-correlation peak, we therefore took advantage of the differences in transfer efficiency of the auto-correlation and sequential transfer during the ^{15}N–$^{13}C_\alpha$ transfer delay T_{NC}. For the sequential peak the transfer efficiency is (Mantylahti et al. 2011)

$$I_{seq} \propto \sin\left(2\pi^1 J_{C\alpha N} T_{NC}\right) \sin\left(2\pi^2 J_{C\alpha N} T_{NC}\right) \quad (1)$$

while the intensity of the auto-correlation peak follows

$$I_{auto} \propto \cos\left(2\pi^1 J_{C\alpha N} T_{NC}\right) \cos\left(2\pi^2 J_{C\alpha N} T_{NC}\right) \quad (2)$$

With $^1J_{C\alpha N}$ and $^2J_{C\alpha N}$ values of 10.6 and 7.5 Hz, respectively, the intensity of the $(i-1)$ to i transfer can be maximized when T_{NC} is set to 25 ms, while at the same time minimizing the auto-correlation transfer (Mantylahti et al. 2011). Proline is an N-substituted amino acid in which the side-chain $^{13}C_\delta$ spin replaces the ^{15}N bound amide proton. Therefore the transfer function is modulated by the additional one-bond coupling between ^{15}N–$^{13}C_\delta$:

$$I_{seq}^{pro} \propto \sin\left(2\pi^1 J_{C\alpha N} T_{NC}\right) \sin\left(2\pi^2 J_{C\alpha N} T_{NC}\right) \cos\left(2\pi^1 J_{C\delta N} T_{NC}\right) \quad (3)$$

As $^1J_{C\delta N}$ is approximately 10.5 Hz, the transfer efficiency for proline residues is close to zero when $T_{NC} = 25$ ms. The signal of prolines could be maximized by setting T_{NC} to ~35 ms. However, this has the disadvantage that overlapping signals might cancel out due to the different signal phases. We therefore chose to set T_{NC} to 25 ms, although this results in the loss of cross-peaks when residue i (i.e. the residue to which the magnetization is transferred in the 6D HCACONCAH) is a proline. Note, however, that H_α, C_α and C' chemical shifts of proline residues are accessible in the 6D HCACONCAH through cross-peaks, where the magnetization originates from the H_α of prolines and is transferred to a succeeding non-proline residue.

Glycine also needs special attention, as it is the only amino acid that does not have a C_β spin and where two

protons are attached to the C_α. During the $^{13}C_\alpha(i)$ and $^{13}C_\alpha(i-1)$ chemical shift evolution periods all residues except glycine are modulated by the homonuclear scalar coupling to C_β according to sin $(2\pi T_{CN} J_{CACB})$ and subsequently become negative with $T_{CN} = 14$ ms. Furthermore, refocusing of anti-phase C–H magnetization should be adjusted for glycine due to its I_2S spin system. For non-glycine residues this delay should optimally be set to 3.4 ms, corresponding to $1/(2J_{CH})$, which would mostly suppresses glycine signals. An often employed compromise is therefore $\tau_2 = 2.4$ ms. However, by setting $\tau_2 = 2.4$ ms and at the same time $T_{CN} = 14$ ms, glycine signals have the opposite phase when compared to other amino acid types. The distinct signal phase from glycine and non-glycine residues can be a useful starting point for manual resonance assignment (Mantylahti et al. 2011). However, it complicates GAPRO peak picking and automatic assignment. We therefore set τ_2 to 4.8 ms resulting in the same phase and good signal-to-noise for both non-glycine and glycine residues. Due to the favorable relaxation properties of IDPs, increased relaxation losses can be largely neglected.

To avoid excessively long measurement times and provide highly accurate chemical shifts, the 6D HCACONCAH experiment was implemented according to the APSY approach, in which indirect chemical shift evolution periods are incremented simultaneously. This results in a set of 2D projections according to a predefined set of projection angles. The 2D projections are then analyzed using the algorithm GAPRO, which performs automatic peak picking on the 2D projections and merges the individual peak lists into a set of six-dimensional spin systems. Although the sensitivity in each 2D projection is limited, detection of correlations in different projections and subsequent averaging results in highly accurate peak positions (Fiorito et al. 2006; Hiller et al. 2005, 2008). The final peak list contains the chemical shifts of $H_\alpha(i-1)$, $C_\alpha(i-1)$, $C'(i-1)$, N(i), $C_\alpha(i)$ and $H_\alpha(i)$, such that the chemical shifts of C_α–$H_\alpha(i-1)$ and C_α–$H_\alpha(i)$ are correlated in a single spin system.

Application of 6D HCACONCAH APSY to α-synuclein

The 6D HCACONCAH APSY experiment was applied to the 140-residue IDP α-synuclein. Figure 2 shows five orthogonal projections of the 6D HCACONCAH APSY recorded on α-synuclein. The projection angles (α, β, γ, δ) were (0, 0, 0, 90), (0, 90, 0, 0), (0, 0, 0, 0), (0, 0, 90, 0) and (90, 0, 0, 0) and result in the $H_\alpha(i-1)$–$H_\alpha(i)$, $C'(i-1)$–$H_\alpha(i)$, $C_\alpha(i)$–$H_\alpha(i)$, $C_\alpha(i-1)$–$H_\alpha(i)$ and N(i)–$H_\alpha(i)$ projections. Signal overlap is most pronounced in the $H_\alpha(i-1)$–

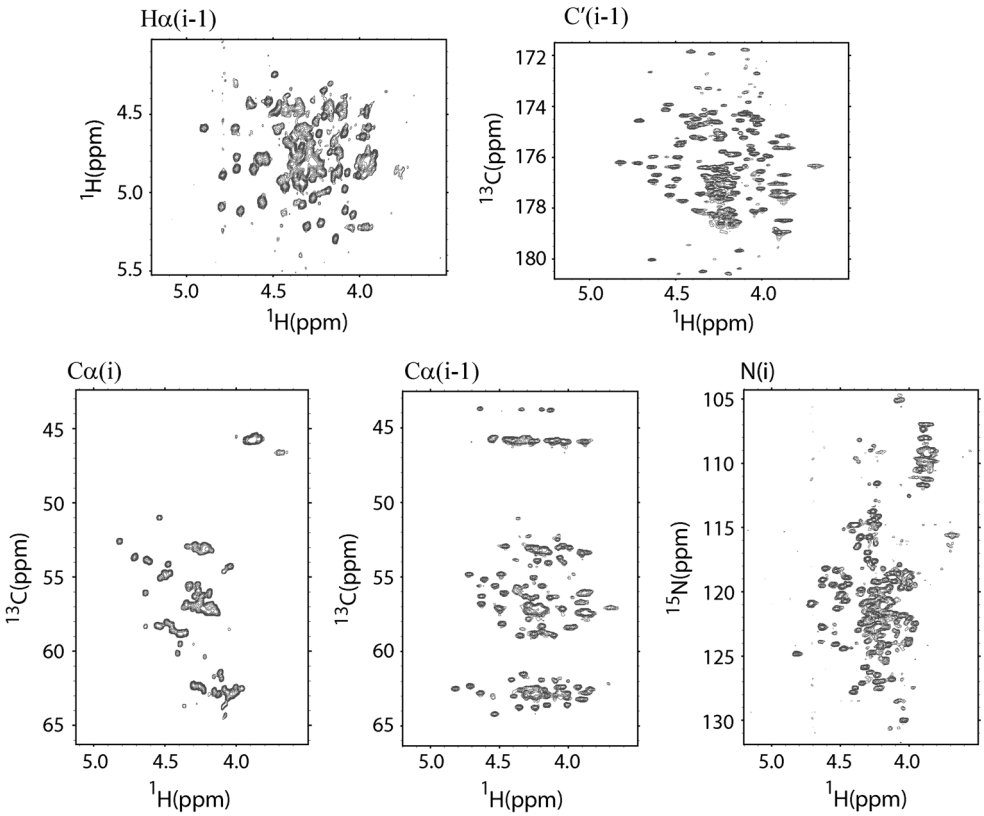

Fig. 2 Orthogonal projection spectra of a 6D HCACONCAH APSY recorded at 700 MHz for α-synuclein at 298 K and pD 6.0. The five projections correspond to the $H_\alpha(i-1)$–$H_\alpha(i)$, $C'(i-1)$–$H_\alpha(i)$, $C_\alpha(i)$–$H_\alpha(i)$, $C_\alpha(i-1)$–$H_\alpha(i)$ and N(i)–$H_\alpha(i)$ planes

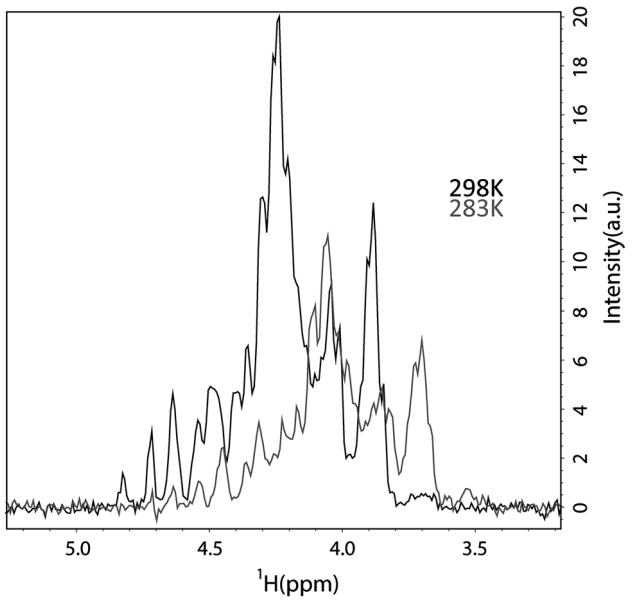

Fig. 3 Influence of temperature on the sensitivity of 6D HCACONCAH APSY. Shown are first serial files recorded for α-synuclein at 298 (*black*) and 283 K (*grey*). The number of scans was 16. The overall temperature-induced shift was not corrected

H_α(i) projection, while the projection of C′(i − 1)–H_α(i) and N(i)–H_α(i) have better chemical shift dispersion, consistent with a larger spread of C′ and N chemical shifts in IDPs. Notably, cross-peaks of glycine residues have the same phase as peaks from other residues as discussed above ($\tau_2 = 4.8$ ms). As the 6D HCACONCAH is not affected by solvent exchange, the sensitivity of the 6D HCACONCAH experiment increased at higher temperatures, consistent with improved relaxation properties at higher temperatures (Fig. 3). Additionally recorded projections combine chemical shifts from several nuclei in the indirect dimension. Analysis of a total of 65 projections (see Supplementary Material Table S1) resulted in a list of 130 six-dimensional spin systems.

The list of 130 six-dimensional spin systems was fed into the software MARS (Jung and Zweckstetter 2004) for automatic sequence-specific assignment. Sequential connectivity is established by correlation of C_α–H_α pairs in different spin systems. Because of the high accuracy of APSY derived chemical shifts, the matching tolerance for the C_α and H_α chemical shifts could be set to very low values—that is 0.05 ppm for C_α and 0.02 ppm for H_α. Without further manual intervention, MARS was able to reliably assign 95 of 135 non-proline residues of α-synuclein. Missing assignments were mostly located at the N-terminus of α-synuclein, which is affected by conformational exchange and has therefore lower signal intensities even in HA-detected experiments. Comparison with the published backbone chemical shifts of α-synuclein

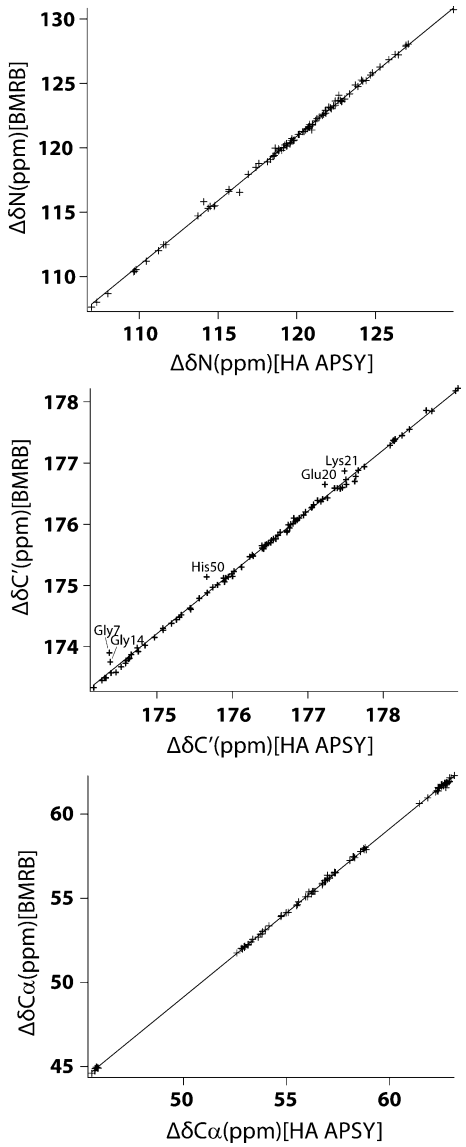

Fig. 4 Comparison of chemical shift assignments of α-synuclein obtained on the basis of the 6D HCACONCAH APSY with published assignments (BMRB ID number: 6968). The 6D HCACONCAH APSY was recorded at 298 K, pD 6.0. Resonance assignments were obtained without manual intervention by feeding 130 six-dimensional spin systems H_α(i − 1)–C_α(i − 1)–C′(i − 1)–N(i)–C_α(i)–H_α(i) into the assignment software MARS (Jung and Zweckstetter 2004). The published assignment of α-synuclein (BMRB ID number: 6968) had been obtained at 285.5 K, pH 6.5. A few residues, for which the C′ chemical shifts deviate, are marked

(BMRB ID number: 6968) pointed to a low error rate (Fig. 4). Gly7 and Gly14 were potentially assigned wrongly by MARS due to the low chemical shift dispersion of C_α and H_α. The change in C′ chemical shift of His50 on the other hand is due to differences in pH and temperature between the current study (pD 6.0, 298 K) and values deposited in the BMRB (pH 6.5, 285.5 K).

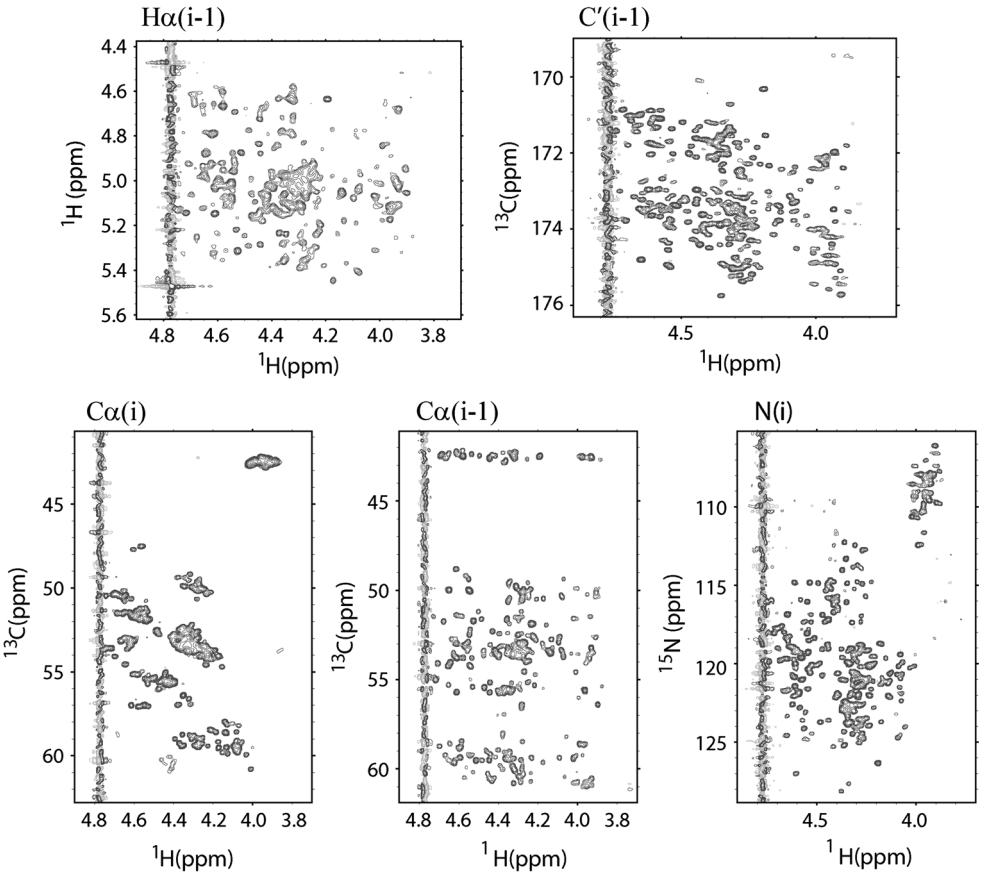

Fig. 5 Orthogonal projection spectra of a 6D HCACONCAH APSY recorded at 900 MHz for htau23 at 298 K, pD 6.8. The five projections correspond to the $H_\alpha(i-1)$–$H_\alpha(i)$, $C'(i-1)$–$H_\alpha(i)$, $C_\alpha(i)$–$H_\alpha(i)$, $C_\alpha(i-1)$–H_α (i) and N(i)–$H_\alpha(i)$ planes. The residual water signal is larger than in the spectra of α-synuclein potentially due to higher water content in the htau23 sample

Application of 6D HCACONCAH APSY to the 352-residue isoform of Tau

To test the applicability of the approach for large IDPs, we recorded the 6D HCACONCAH APSY experiment on the 352-residue isoform of Tau, htau23. Tau is a microtubule-associated protein that plays a key role in Alzheimer's disease (Braak and Braak 1991). 65 projections including 5 orthogonal projections (Fig. 5; Supplementary Material Table S1) were recorded in 84 h. GAPRO analysis of the projections resulted in 291 six-dimensional spin systems. Based on the 6D HCACONCAH derived spin systems, MARS obtained 237 assignments, classified by MARS as reliable, for 318 non-proline residues. We then compared the assignments with those previously determined by us for htau23 using 5- and 7-dimensional HN-detected APSY experiments (Narayanan et al. 2010). Figure 6 shows that most assignments where the chemical shifts deviated from those, which were previously determined, are associated with assignments classified by MARS as low reliable (grey bars). Other residues that had chemical shift differences were His14, Ala15, His32, Glu47, His63, Lys83, His210, Thr284, His299 and His318. We attribute the change in chemical shift of histidine residues to the difference in pH between the two studies: HN-detected APSY experiments were recorded at pH 6.0 while the 6D HCACONCAH APSY was recorded at pH 6.8 (in order to demonstrate that the experiment also works at a pH where solvent exchange in IDP profoundly affects HN-detection). Deviations for other residues might also be influenced by the difference in pH or might be due to incorrect assignments made by the MARS program in either the HN or HA-detected APSY experiment.

Discussion

6D HCACONCAH APSY enables the acquisition of high-dimensional chemical shift correlations through simultaneous chemical shift labeling of multiple indirect dimensions. The six different chemical shifts $H_\alpha(i-1)$, $C_\alpha(i-1)$, $C'(i-1)$, N(i), $C_\alpha(i)$ and $H_\alpha(i)$ are correlated in a single cross peak (Fig. 1a), such that two spin systems can be connected sequentially by employing both the H_α and C_α chemical shift. The experiment was designed to specifically provide sequential correlation and to suppress undesired intra-residue magnetization transfer (Fig. 1b). In this way spectral overlap is minimized and chemical shift ambiguity

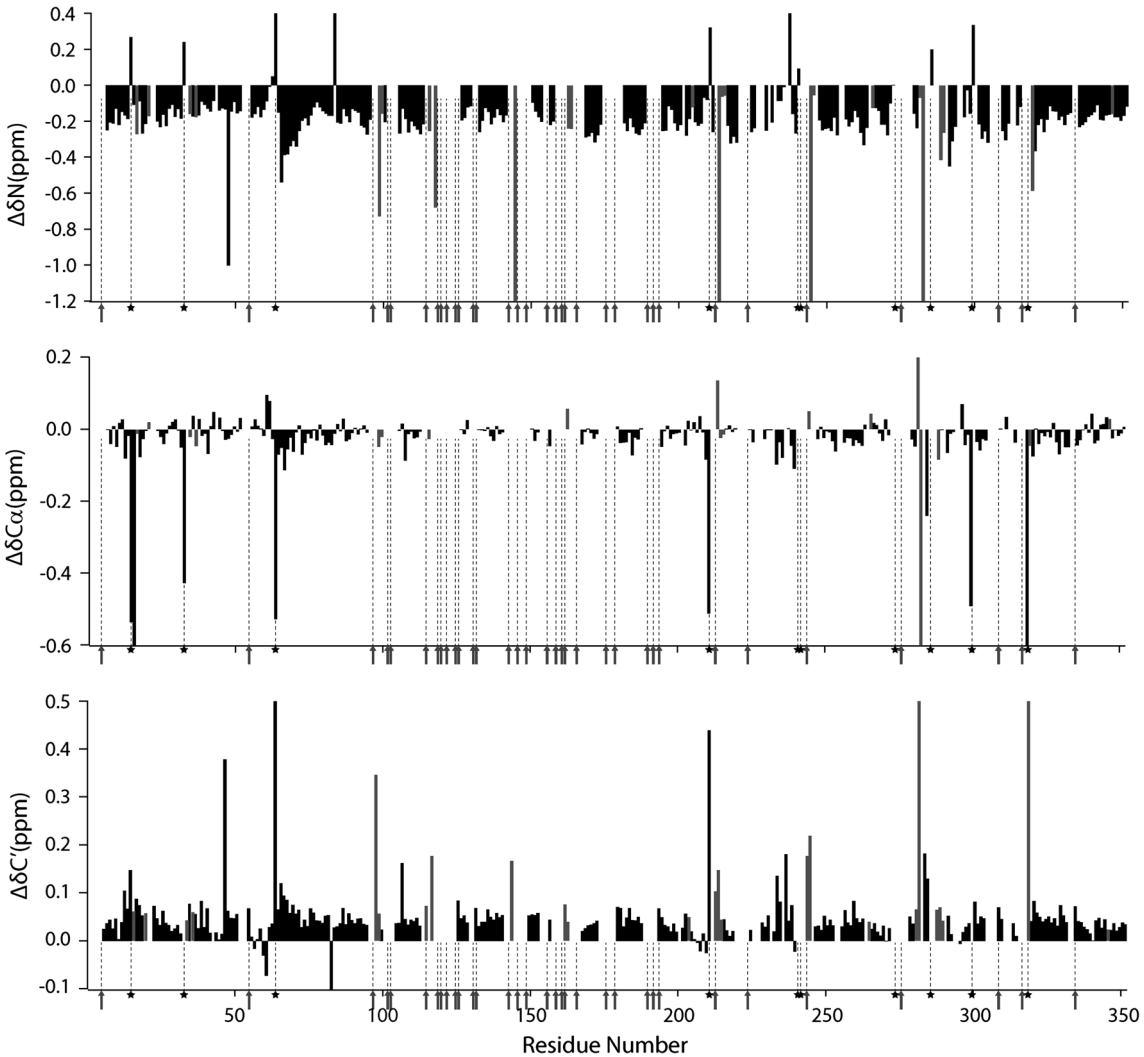

Fig. 6 Chemical shift differences between assignments obtained by MARS on the basis of the 6D HCACONCAH APSY (this study) and previous assignments obtained by MARS for htau23 using a combination of 5D and 7D HN-detected APSY experiments (Narayanan et al. 2010). Residues, for which the assignment was classified by MARS as high and medium reliable (Jung and Zweckstetter 2004) are shown by *black bars*, *grey bars* show the chemical shift difference for assignments classified by MARS as low reliable. Proline and histidine residues are indicated by *arrows* and *stars*, respectively. Note that the 6D HCACONCAH APSY was recorded at 298 K, pD 6.8, while previous HN-based assignments were obtained at 298 K, pD 6.0, resulting in a slight overall offset in the ^{15}N and C′ dimension, as well as chemical shift changes for histidine residues and residues in proximity to histidines

is avoided for efficient automatic resonance assignment (Figs. 2, 5). As the H_α magnetization is used for detection, problems with rapid exchange of amide protons, which attenuates signal intensities in HN-detected experiments at pH values above ~6.2, are avoided. This enables measurement of the 6D HCACONCAH APSY at higher temperatures. Indeed, because of improved relaxation properties the sensitivity of the 6D HCACONCAH APSY increases with increasing temperatures (Fig. 3).

Application of the 6D HCACONCAH APSY to two intrinsically disordered proteins, 140-residue α-synuclein and 352-residue htau23, demonstrated that the chemical shift correlations provided by 6D HCACONCAH APSY are highly useful for automatic backbone resonance assignment (Figs. 4, 6). Depending on protein concentration, the experiment can be recorded in 60–85 h. Combined with automatic peak picking as implemented in GAPRO and automatic assignment using the software MARS, backbone resonance assignment of intrinsically disordered proteins can be performed efficiently. This is in agreement with previous findings that the assignment of IDPs, including those with a long primary sequence and high sequence degeneration, can be reliably assigned by automatic methods (Narayanan et al. 2010).

The 6D HCACONCAH APSY can be combined with other HA-detected experiments, in particular those

optimized for proline-rich sequences such as 3D HACAN and 3D HACA(CO)N (Kanelis et al. 2000). In case solvent exchange is not too strong, the combination of 6D HCACONCAH APSY with 5D HACACONH APSY is likely to be useful. HN chemical shifts might also be accessed through a 3D HNCO experiment, which has quite good resolution even for IDPs, is the most sensitive triple-resonance experiment and can either use HN-detection or ^{13}C-detection (Hu et al. 2007). Alternatively, H_N and C_β chemical shifts might be determined with the help of a 5D CBCACONH APSY (Hiller et al. 2008). In addition, manual inspection of the spectra might further increase the quality of assignment. Similar to other 5–7 dimensional experiments, the 6D HCACONCAH APSY is most suited for proteins with favorable relaxation properties such as IDPs.

Conclusion

We presented a six-dimensional alpha proton detection-based APSY experiment for backbone assignment of intrinsically disordered proteins. The 6D HCACONCAH APSY correlates six different chemical shifts, $H_\alpha(i-1)$, $C_\alpha(i-1)$, $C'(i-1)$, N(i), $C_\alpha(i)$ and $H_\alpha(i)$, and allows efficient backbone resonance assignment of intrinsically disordered proteins in conditions where solvent exchange interferes with HN-detected experiments.

Acknowledgments We thank Eckhard Mandelkow and Jacek Biernat for the htau23 sample. This work was in part supported by the DFG through ZW71/3-2 and ZW71/7-1.

References

Atreya HS, Szyperski T (2004) G-matrix Fourier transform NMR spectroscopy for complete protein resonance assignment. Proc Natl Acad Sci USA 101:9642–9647. doi:10.1073/pnas.0403529101

Barna JCJ, Laue ED, Mayger MR, Skilling J, Worrall SJP (1987) Exponential sampling, an alternative method for sampling in two-dimensional NMR experiments. J Magn Reson 73:69–77. doi:10.1016/0022-2364(87)90225-3

Bermel W, Bertini I, Felli IC, Kummerle R, Pierattelli R (2006a) Novel 13C direct detection experiments, including extension to the third dimension, to perform the complete assignment of proteins. J Magn Reson 178:56–64. doi:10.1016/j.jmr.2005.08.011

Bermel W, Bertini I, Felli IC, Lee YM, Luchinat C, Pierattelli R (2006b) Protonless NMR experiments for sequence-specific assignment of backbone nuclei in unfolded proteins. J Am Chem Soc 128:3918–3919. doi:10.1021/Ja0582206

Bermel W, Bertini I, Chill J, Felli IC, Haba N, Kumar MVV, Pierattelli R (2012a) Exclusively heteronuclear C-13-Detected amino-acid-selective NMR experiments for the study of intrinsically disordered proteins (IDPs). Chembiochem 13:2425–2432. doi:10.1002/cbic.201200447

Bermel W et al (2012b) Speeding up sequence specific assignment of IDPs. J Biomol NMR 53:293–301. doi:10.1007/s10858-012-9639-0

Bermel W, Felli IC, Gonnelli L, Kozminski W, Piai A, Pierattelli R, Zawadzka-Kazimierczuk A (2013) High-dimensionality 13C direct-detected NMR experiments for the automatic assignment of intrinsically disordered proteins. J Biomol NMR 57:353–361. doi:10.1007/s10858-013-9793-z

Bertini I, Duma L, Felli IC, Fey M, Luchinat C, Pierattelli R, Vasos PR (2004) A heteronuclear direct-detection NMR spectroscopy experiment for protein-backbone assignment. Angew Chem Int Edit 43:2257–2259. doi:10.1002/anie.200453661

Bottomley MJ, Macias MJ, Liu Z, Sattler M (1999) A novel NMR experiment for the sequential assignment of proline residues and proline stretches in 13C/15 N-labeled proteins. J Biomol NMR 13:381–385

Braak H, Braak E (1991) Neuropathological stageing of Alzheimer-related changes. Acta Neuropathol 82:239–259

Chylla RA, Markley JL (1995) Theory and application of the maximum likelihood principle to NMR parameter estimation of multidimensional NMR data. J Biomol NMR 5:245–258

Coggins BE, Zhou P (2006) Polar Fourier transforms of radially sampled NMR data. J Magn Reson 182:84–95. doi:10.1016/j.jmr.2006.06.016

Coggins BE, Venters RA, Zhou P (2004) Generalized reconstruction of n-D NMR spectra from multiple projections: application to the 5-D HACACONH spectrum of protein G B1 domain. J Am Chem Soc 126:1000–1001. doi:10.1021/ja039430q

Croke RL, Sallum CO, Watson E, Watt ED, Alexandrescu AT (2008) Hydrogen exchange of monomeric alpha-synuclein shows unfolded structure persists at physiological temperature and is independent of molecular crowding in *Escherichia coli*. Protein Sci 17:1434–1445. doi:10.1110/ps.033803.107

Csizmok V, Felli IC, Tompa P, Banci L, Bertini I (2008) Structural and dynamic characterization of intrinsically disordered human securin by NMR spectroscopy. J Am Chem Soc 130:16873–16879. doi:10.1021/ja805510b

Felli IC, Brutscher B (2009) Recent advances in solution NMR: fast methods and heteronuclear direct detection. Chemphyschem 10:1356–1368. doi:10.1002/cphc.200900133

Fiorito F, Hiller S, Wider G, Wuthrich K (2006) Automated resonance assignment of proteins: 6D APSY-NMR. J Biomol NMR 35:27–37. doi:10.1007/s10858-006-0030-x

Güntert P, Dötsch V, Wider G, Wüthrich K (1992) Processing of multidimensional NMR data with the new software PROSA. J Biomol NMR 2:619–629. doi:10.1007/Bf02192850

Hiller S, Fiorito F, Wuthrich K, Wider G (2005) Automated projection spectroscopy (APSY). Proc Natl Acad Sci USA 102:10876–10881. doi:10.1073/pnas.0504818102

Hiller S, Wider G, Wuthrich K (2008) APSY-NMR with proteins: practical aspects and backbone assignment. J Biomol NMR 42:179–195. doi:10.1007/s10858-008-9266-y

Holland DJ, Bostock MJ, Gladden LF, Nietlispach D (2011) Fast multidimensional NMR spectroscopy using compressed sensing. Angew Chem Int Edit 50:6548–6551. doi:10.1002/Anie.201100440

Hu K, Vogeli B, Clore GM (2007) Spin-state selective carbon-detected HNCO with TROSY optimization in all dimensions and double echo-antiecho sensitivity enhancement in both indirect dimensions. J Am Chem Soc 129:5484–5491. doi:10.1021/ja0679811

Iakoucheva LM, Brown CJ, Lawson JD, Obradovic Z, Dunker AK (2002) Intrinsic disorder in cell-signaling and cancer-associated proteins. J Mol Biol 323:573–584

Jensen MR, Ruigrok RW, Blackledge M (2013) Describing intrinsically disordered proteins at atomic resolution by NMR. Curr Opin Struct Biol 23:426–435. doi:10.1016/j.sbi.2013.02.007

Jung YS, Zweckstetter M (2004) Mars—robust automatic backbone assignment of proteins. J Biomol NMR 30:11–23. doi:10.1023/B:JNMR.0000042954.99056.ad

Kanelis V, Donaldson L, Muhandiram DR, Rotin D, Forman-Kay JD, Kay LE (2000) Sequential assignment of proline-rich regions in proteins: application to modular binding domain complexes. J Biomol NMR 16:253–259. doi:10.1023/A:1008355012528

Kay LE, Keifer P, Saarinen T (1992) Pure absorption gradient enhanced heteronuclear single quantum correlation spectroscopy with improved sensitivity. J Am Chem Soc 114:10663–10665. doi:10.1021/Ja00052a088

Kazimierczuk K, Orekhov VY (2011) Accelerated NMR spectroscopy by using compressed sensing. Angew Chem Int Ed Engl 50:5556–5559. doi:10.1002/anie.201100370

Kazimierczuk K, Kozminski W, Zhukov I (2006) Two-dimensional Fourier transform of arbitrarily sampled NMR data sets. J Magn Reson 179:323–328. doi:10.1016/j.jmr.2006.02.001

Kazimierczuk K, Stanek J, Zawadzka-Kazimierczuk A, Kozminski W (2013) High-dimensional NMR spectra for structural studies of biomolecules. Chemphyschem 14:3015–3025. doi:10.1002/cphc.201300277

Kim S, Szyperski T (2003) GFT NMR, a new approach to rapidly obtain precise high-dimensional NMR spectral information. J Am Chem Soc 125:1385–1393. doi:10.1021/Ja028197d

Korzhneva DM, Ibraghimov IV, Billeter M, Orekhov VY (2001) MUNIN: application of three-way decomposition to the analysis of heteronuclear NMR relaxation data. J Biomol NMR 21:263–268

Kupce E, Freeman R (2003a) Projection-reconstruction of three-dimensional NMR spectra. J Am Chem Soc 125:13958–13959. doi:10.1021/Ja038297z

Kupce E, Freeman R (2003b) Reconstruction of the three-dimensional NMR spectrum of a protein from a set of plane projections. J Biomol NMR 27:383–387

Kupce E, Freeman R (2004) Projection-reconstruction technique for speeding up multidimensional NMR spectroscopy. J Am Chem Soc 126:6429–6440. doi:10.1021/ja049432q

Mantylahti S, Aitio O, Hellman M, Permi P (2010) HA-detected experiments for the backbone assignment of intrinsically disordered proteins. J Biomol NMR 47:171–181. doi:10.1007/s10858-010-9421-0

Mantylahti S, Hellman M, Permi P (2011) Extension of the HA-detection based approach: (HCA)CON(CA)H and (HCA)NCO(CA)H experiments for the main-chain assignment of intrinsically disordered proteins. J Biomol NMR 49:99–109. doi:10.1007/s10858-011-9470-z

Marsh JA, Forman-Kay JD (2010) Sequence determinants of compaction in intrinsically disordered proteins. Biophys J 98:2383–2390. doi:10.1016/j.bpj.2010.02.006

Mccoy MA, Mueller L (1992) Nonresonant effects of frequency-selective pulses. J Magn Reson 99:18–36. doi:10.1016/0022-2364(92)90152-W

Mittag T, Forman-Kay JD (2007) Atomic-level characterization of disordered protein ensembles. Curr Opin Struct Biol 17:3–14. doi:10.1016/j.sbi.2007.01.009

Motackova V et al (2010) Strategy for complete NMR assignment of disordered proteins with highly repetitive sequences based on resolution-enhanced 5D experiments. J Biomol NMR 48:169–177. doi:10.1007/s10858-010-9447-3

Narayanan RL, Durr UH, Bibow S, Biernat J, Mandelkow E, Zweckstetter M (2010) Automatic assignment of the intrinsically disordered protein Tau with 441-residues. J Am Chem Soc 132:11906–11907. doi:10.1021/ja105657f

Novacek J et al (2011) 5D 13C-detected experiments for backbone assignment of unstructured proteins with a very low signal dispersion. J Biomol NMR 50:1–11. doi:10.1007/s10858-011-9496-2

Novacek J, Janda L, Dopitova R, Zidek L, Sklenar V (2013) Efficient protocol for backbone and side-chain assignments of large, intrinsically disordered proteins: transient secondary structure analysis of 49.2 kDa microtubule associated protein 2c. J Biomol NMR 56:291–301. doi:10.1007/s10858-013-9761-7

Orekhov VY, Ibraghimov IV, Billeter M (2001) MUNIN: a new approach to multi-dimensional NMR spectra interpretation. J Biomol NMR 20:49–60

Pervushin K, Eletsky A (2003) A new strategy for backbone resonance assignment in large proteins using a MQ-HACACO experiment. J Biomol NMR 25:147–152

Rezaei-Ghaleh N, Blackledge M, Zweckstetter M (2012) Intrinsically disordered proteins: from sequence and conformational properties toward drug discovery. Chembiochem 13:930–950. doi:10.1002/cbic.201200093

Shen Y, Atreya HS, Liu GH, Szyperski T (2005) G-matrix Fourier transform NOESY-based protocol for high-quality protein structure determination. J Am Chem Soc 127:9085–9099. doi:10.1021/Ja0501870

Shimba N et al (2004) Optimization of 13C direct detection NMR methods. J Biomol NMR 30:175–179. doi:10.1023/B:JNMR.0000048855.35771.11

Skora L, Becker S, Zweckstetter M (2010) Molten globule precursor states are conformationally correlated to amyloid fibrils of human beta-2-microglobulin. J Am Chem Soc 132:9223–9225. doi:10.1021/ja100453e

Szyperski T, Atreya HS (2006) Principles and applications of GFT projection NMR spectroscopy. Magn Reson Chem 44:51–60. doi:10.1002/mrc.1817

Takeuchi K, Frueh DP, Hyberts SG, Sun ZY, Wagner G (2010) High-resolution 3D CANCA NMR experiments for complete main-chain assignments using Cα direct detection. J Am Chem Soc 132:2945–2951. doi:10.1021/ja907717b

Tompa P (2002) Intrinsically unstructured proteins. Trends Biochem Sci 27:527–533

Uversky VN (2002) Natively unfolded proteins: a point where biology waits for physics. Protein Sci 11:739–756. doi:10.1110/ps.4210102

Uversky VN (2011) Flexible nets of malleable guardians: intrinsically disordered chaperones in neurodegenerative diseases. Chem Rev 111:1134–1166. doi:10.1021/cr100186d

Uversky VN, Oldfield CJ, Dunker AK (2008) Intrinsically disordered proteins in human diseases: introducing the D2 concept. Annu Rev Biophys 37:215–246. doi:10.1146/annurev.biophys.37.032807.125924

Wang AC, Grzesiek S, Tschudin R, Lodi PJ, Bax A (1995) Sequential backbone assignment of isotopically enriched proteins in D2O by deuterium-decoupled HA(CA)N and HA(CACO)N. J Biomol NMR 5:376–382

Wilkins DK, Grimshaw SB, Receveur V, Dobson CM, Jones JA, Smith LJ (1999) Hydrodynamic radii of native and denatured proteins measured by pulse field gradient NMR techniques. Biochemistry 38:16424–16431. doi:10.1021/Bi991765q

Wright PE, Dyson HJ (1999) Intrinsically unstructured proteins: re-assessing the protein structure-function paradigm. J Mol Biol 293:321–331. doi:10.1006/jmbi.1999.3110

Zawadzka-Kazimierczuk A, Kozminski W, Billeter M (2012a) TSAR: a program for automatic resonance assignment using 2D cross-sections of high dimensionality, high-resolution spectra. J Biomol NMR 54:81–95. doi:10.1007/s10858-012-9652-3

Zawadzka-Kazimierczuk A, Kozminski W, Sanderova H, Krasny L (2012b) High dimensional and high resolution pulse sequences for backbone resonance assignment of intrinsically disordered proteins. J Biomol NMR 52:329–337. doi:10.1007/s10858-012-9613-x